Journal of Power Sources 222 (2013) 196–201

Contents lists available at SciVerse ScienceDirect

Journal of Power Sources

journal homepage: www.elsevier.com/locate/jpowsour

Short communication

$Li_4Ti_5O_{12}$–TiO_2 composite anode material for lithium-ion batteries

Jie Wang [a], Hailei Zhao [a,b,*], Qian Yang [a], Chunmei Wang [a], Pengpeng Lv [a], Qing Xia [a]

[a] School of Materials Science and Engineering, University of Science and Technology Beijing, Beijing 100083, China
[b] Beijing Key Lab of New Energy Materials and Technologies, Beijing 100083, China

HIGHLIGHTS

- Dual-phase $Li_4Ti_5O_{12}$–TiO_2 was *in situ* prepared by a solvothermal route.
- TiO_2 can prevent the grain growth and particle aggregation of $Li_4Ti_5O_{12}$ phase.
- $Li_4Ti_5O_{12}$–TiO_2 powder displays high specific capacity and good cycling performance.
- Carbon coated $Li_4Ti_5O_{12}$–TiO_2 exhibits an excellent rate-capability.

ARTICLE INFO

Article history:
Received 16 July 2012
Received in revised form
19 August 2012
Accepted 29 August 2012
Available online 7 September 2012

Keywords:
Lithium titanium oxide
Anode material
Electrochemical properties
Lithium-ion battery
Rate-capability

ABSTRACT

In an effort to improve the rate-capability of $Li_4Ti_5O_{12}$ anode material, a dual-phase composite $Li_4Ti_5O_{12}$–TiO_2 is *in situ* prepared via a solvothermal route. The $Li_4Ti_5O_{12}$–TiO_2 composite shows higher reversible capacity and better rate-capability compared to single phase $Li_4Ti_5O_{12}$. The TiO_2 can decrease significantly the particle size of $Li_4Ti_5O_{12}$–TiO_2 powders due to a steric hindrance effect, which thereby shortens the lithium ion diffusion distance and enhances the electrode reaction. Meanwhile, anatase TiO_2 can contribute some capacity to the $Li_4Ti_5O_{12}$–TiO_2 electrode. Coating the $Li_4Ti_5O_{12}$–TiO_2 composite with carbon (~2.5 wt.%) can further improve the rate-capability of $Li_4Ti_5O_{12}$–TiO_2 electrode, a reversible capacity of ~140 mA h g^{-1} is maintained after 100 cycles at 5 C.

1. Introduction

The appearance of lithium-ion batteries has changed the human daily life-style significantly, which was widely used as the key energy component of the digital products in today's information society due to the advantages of higher energy density, higher working voltage, and even the friendliness toward the environment [1–3]. In order to meet the demand of electric vehicles (EV) on power sources, many efforts have been made to develop new active electrode materials with high specific energy density and excellent power performance [4]. Graphite-based material was commonly used as the anode material in the state-of-the-art lithium-ion batteries due to its desirable charge potential profile, good cycleability and safety features, and abundant reserves in natural world. However, it suffers from the poor rate-capability, co-intercalation of solvated lithium ion due to its layered structural characteristics, and lower lithiation potential (close to 0 V vs. Li^+/Li), which may cause the dendritic deposition of metal lithium on the electrode surface if the batteries are over-charged, limiting the application in power battery for EV development [5]. Therefore, searching for alternative anode materials with excellent rate-capability and good safety property has become the main topic in the battery research field. Many new anode materials have been proposed and extensively investigated, such as Sn-based, Sb-based and Si-based materials [5–8], various transition metal oxides [9–14], hard carbons [6], and $Li_4Ti_5O_{12}$ [15,16].

In particular, $Li_4Ti_5O_{12}$ is of interest as the anode material for lithium-ion batteries used for EV and energy storage devices owing to its favorable characteristics, including good structure stability ("zero strain" material) during lithium insertion/extraction process and higher flat electrode reaction voltage (1.55 V vs. Li^+/Li). The former ensures the long-term cycling stability, while the latter enables the reliable safety [16–18]. Both are urgently desired for EV and energy storage systems. Although the operating voltage of

* Corresponding author. School of Materials Science and Engineering, University of Science and Technology Beijing, Beijing 100083, China. Tel./fax: +86 10 82376837.
E-mail address: hlzhao@ustb.edu.cn (H. Zhao).

0378-7753/$ – see front matter © 2012 Elsevier B.V. All rights reserved.
http://dx.doi.org/10.1016/j.jpowsour.2012.08.082

$Li_4Ti_5O_{12}$ is higher than other anode candidate materials, it still can be coupled with $LiMn_2O_4$, $Li[Ni_{1/2}Mn_{3/2}]O_4$, or $LiCoO_2$ cathode materials having high voltage to provide a cell with the voltage 2.5–3.0 V [19,20].

Despite of these advantages, $Li_4Ti_5O_{12}$ still suffers from its extremely low electronic conductivity and unsatisfactory lithium ionic conductivity, which seriously limit the rate-capability. Many strategies have been employed to enhance the electronic and ionic conductivities of $Li_4Ti_5O_{12}$ anode material with the aim of improving its rate-capability. Lattice doping with aliovalent cations [21–24] and simply introducing a second phase with high electronic conductivity, such as Ag, Cu, C, CNTs, graphene [25–29], can both increase the electronic conductivity. The preparation of nanostructured $Li_4Ti_5O_{12}$ has been proved to be an effective way to improve the ionic conductivity of electrode. The nano-sized particles can not only shorten the lithium diffusion distance but also enlarge the specific surface area of active material contacting with electrolyte, which will decrease the local current density of active material and thereby reduce the electrode polarization, resulting in the enhancement of rate-capability of electrode [4].

Nano-sized TiO_2 is a kind of attractive anode material, which has fast lithium insertion/extraction ability and lower volume change during the charge/discharge process [30]. It shows higher electronic conductivity [31] than $Li_4Ti_5O_{12}$ material [21]. The $Li_4Ti_5O_{12}$–TiO_2 composite is attracted much attention most recently as anode material for lithium ion batteries [32,33]. The composite $Li_4Ti_5O_{12}$–rutile TiO_2 was reported by Guo *et al.* [32], which shows better rate-capability than pure $Li_4Ti_5O_{12}$. Rahman *et al.* synthesized composite $Li_4Ti_5O_{12}$–TiO_2 via molten salt method [33], which yields a good electrochemical performance. The high specific capacity of composite $Li_4Ti_5O_{12}$–TiO_2 is deemed to stem from the increased grain-boundary density compared to single phase $Li_4Ti_5O_{12}$.

Various methods have been attempted to prepare nano-sized $Li_4Ti_5O_{12}$, such as sol–gel [34], hydrothermal [32], and solution-combustion [35]. The high specific surface area makes the nano-sized particles tend to aggregate, forming large second-particles and thus losing the nano-particle features. In this work, we propose a new strategy, preparing *in situ* a dual-phase nano-sized composite $Li_4Ti_5O_{12}$–TiO_2 via a simple solvothermal route, where TiO_2 as second and competitive phase can prevent the grain growth and particle aggregation of $Li_4Ti_5O_{12}$ phase. Due to the *in situ* formation feature, the TiO_2 and $Li_4Ti_5O_{12}$ phases can mix homogeneously each other. Taking the fact into account that anatase TiO_2 has a large lattice space along *c*-direction (9.51 Å) compared to rutile [36], which enables the fast lithium ion diffusion through anatase TiO_2. Therefore, the composite $Li_4Ti_5O_{12}$–TiO_2 (anatase) was *in situ* synthesized in this work and expected to have superior electrochemical properties, especially the rate-capability, than single phase $Li_4Ti_5O_{12}$. To further enhance the electronic conductivity, carbon coated $Li_4Ti_5O_{12}$–TiO_2 was also prepared. The structural characteristics and electrochemical properties of $Li_4Ti_5O_{12}$, $Li_4Ti_5O_{12}$–TiO_2 and $Li_4Ti_5O_{12}$–TiO_2/C anode materials were evaluated and compared. The $Li_4Ti_5O_{12}$–TiO_2/C composite exhibits excellent rate-capability and cycling stability.

2. Experimental

2.1. Synthesis

$Li_4Ti_5O_{12}$–TiO_2 (LTO–TO) and $Li_4Ti_5O_{12}$ (LTO) powders were synthesized by a facile solvothermal method combined with a further heat-treatment. $Ti(OC_4H_9)_4$, used as Ti source, was dispersed in 50 ml ethanol under magnetic stirring, then LiAc was added into the transparent solution. The concentration of $Ti(OC_4H_9)_4$ in ethanol was 1.4×10^{-4} mol ml^{-1}. Subsequently, 2 ml ammonia solution (25–28 wt.%) was added drop-wise under stirring to achieve a milky white suspension, which was then transferred to a 100 ml Teflon-lined autoclave for solvothermal treatment at 180 °C for 24 h. After cooling down to room temperature naturally, white precipitate was collected by centrifugation and washed with absolute ethyl ethanol for several times. After drying at 80 °C for 3 h, the precursor was calcined at 600 °C for 2 h in air atmosphere to produce $Li_4Ti_5O_{12}$–TiO_2 composite. Without the addition of ammonia, the pure $Li_4Ti_5O_{12}$ can be prepared with the same procedure.

With respect to the synthesis of carbon-coated $Li_4Ti_5O_{12}$–TiO_2, the calcined $Li_4Ti_5O_{12}$–TiO_2 powder was dispersed into the aqueous solution of sucrose with the mass ratio of ($Li_4Ti_5O_{12}$–TiO_2) to carbon at 97.5/2.5, supposing all the carbon in sucrose ($C_{12}H_{22}O_{11}$) can be obtained via pyrolysis. The solution was dried in a rotary evaporation under reflux condition to let sucrose deposit uniformly on the particle surface of $Li_4Ti_5O_{12}$ and TiO_2. The resultant powder was pyrolyzed at 600 °C for 1 h in nitrogen atmosphere to achieve $Li_4Ti_5O_{12}$–TiO_2/C composite. For simplicity, $Li_4Ti_5O_{12}$, $Li_4Ti_5O_{12}$–TiO_2 and $Li_4Ti_5O_{12}$–TiO_2/C samples are noted as LTO, LTO–TO and LTO–TO/C, respectively.

2.2. Characterization

The chemical composition and crystalline phase of $Li_4Ti_5O_{12}$ and $Li_4Ti_5O_{12}$–TiO_2 were identified by the powder X-ray diffraction (XRD) using Rigaku D/MAX-A diffractometer equipped with Cu Kα radiation source (λ=1.54056 Å) in the 2θ range of 10°–90°. The morphology of the samples was observed by field emission scanning electron microscope (FESEM, SUPRA55) operated at 10 kV. The exact phase composition and the lattice structures of the particles were characterized by using high resolution transmission electron microscopy (HRTEM FEI F20) operated at an accelerating voltage of 200 kV combined with scanning area electron diffraction (SAED) measurement.

2.3. Electrochemical measurement

The electrochemical characteristics of the synthesized three samples were evaluated by using cells. The working electrode was prepared by mixing 85 wt.% active material (LTO, LTO–TO or LTO–TO/C), 10 wt.% acetylene black (AB) as conducting agent and 5 wt.% polyvinylidene fluoride (PVdF) as binder in *N*-methyl pyrrolidinone (NMP). The slurry was spread uniformly on a copper foil. After drying in a vacuum environment at 80 °C for 6 h, the copper foil with electrode materials was punched into circular discs with 8 mm diameter. The circular discs were dried again at 120 °C in vacuum for 24 h. The test cells were assembled in an argon-filled glove box with metal lithium foil as counter electrode, Celgard 2400 microporous membrane as separator and 1 M $LiPF_6$ (1 M) in a mixture of ethylene carbonate (EC), dimethyl-carbonate (DMC), and ethyl methyl carbonate (EMC) with a volume ratio of 1:1:1 as electrolyte. Galvanostatic cycling was conducted on a computer controlled Land CT2001A battery test system at different current densities in the potential range of 1.0–2.5 V. The cyclic voltammogram test was carried out to examine the electrode reaction under the scan rate of 0.01 mV s^{-1} with the voltage ranging of 1.0–3.0 V by using 3-electrode cell.

3. Results and discussion

The XRD patterns of the synthesized samples LTO and LTO–TO are presented in Fig. 1. The diffraction peaks of sample LTO (Fig. 1(a)) can be indexed well to the cubic spinel $Li_4Ti_5O_{12}$ structure (space group *Fd*3*m*) with a lattice constant of 8.371 Å. The second

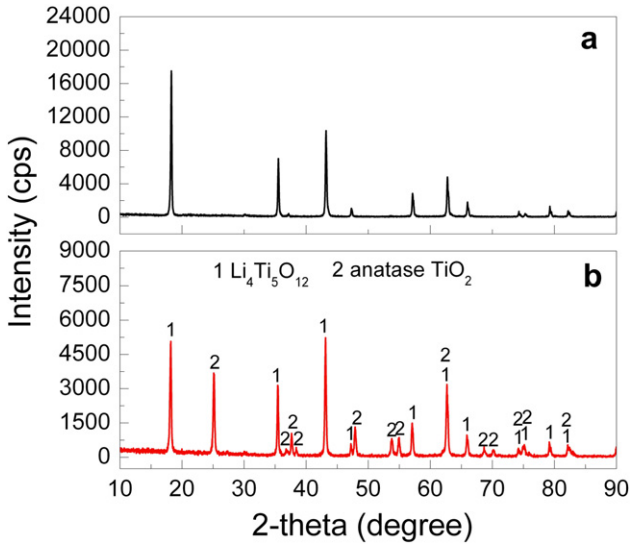

Fig. 1. XRD patterns of the synthesized samples (a) LTO and (b) LTO–TO.

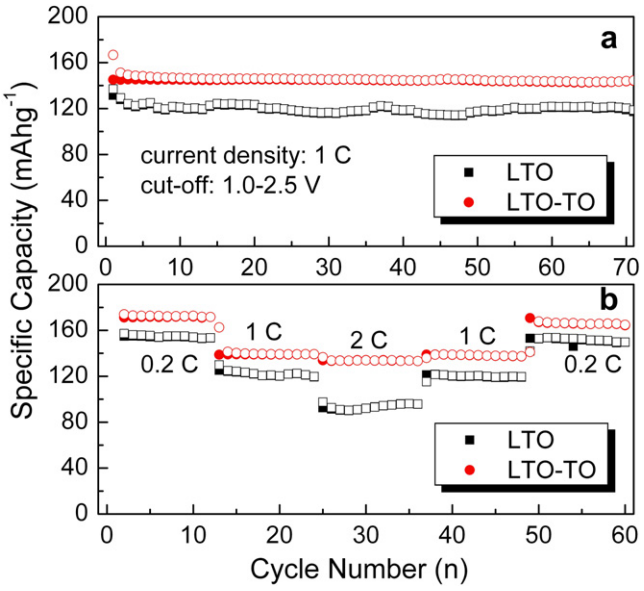

Fig. 3. Cycling performance (a) and stepped cycling performance at different current densities (b) for samples LTO and LTO–TO.

phase appeared upon the addition of ammonia, and the peaks corresponding to the second phase can be well identified as anatase TiO_2 with space group *I*41/*amd*. No other impurity peaks can be observed. Compared to the sample LTO, sample LTO–TO shows lower XRD peak intensity, most probably due to the different particle sizes. Small particle size usually corresponds to weak XRD peak owing to the high specific surface area and the poor lattice arrangement at the particle surface.

The conjecture about the particle size from XRD results is confirmed by FESEM observation. As shown in Fig. 2, sample LTO exhibits spherical particle shape with particle size of ca. 1–2 μm, which is much larger than that of sample LTO–TO, ca. 200–300 nm. Moreover, the *in situ* synthesized composite LTO–TO displays more uniform particle distribution, while sample LTO presents a relatively wide range in particle size distribution and an obvious particle aggregation. This indicates that the second phase TiO_2 plays an important role in preventing the grain growth and particle aggregation, possibly due to the competitive crystallization behavior between LTO and TO particles and the steric hindrance effect. The LTO–TO sample with small particle size and homogeneous particle distribution is expected to have better electrochemical performance.

To investigate the cycling performance of samples LTO and LTO–TO, the galvanostatic discharge/charge cycling measurement was carried out, and the results are shown in Fig. 3. At the current density of 1 C (1 C=175 m Ag^{-1}), sample LTO–TO exhibits high specific capacity and good cycling performance compared to sample LTO. After 70 cycles, the reversible capacity of 145 and 120 mA h g^{-1} is achieved for samples LTO–TO and LTO, respectively, indicating the good electrochemical performance of LTO–TO composite.

To further have an observation on the rate-capability of each sample, the stepped cycling performances at different current densities were examined. The results are shown in Fig. 3(b). The dual-phase sample LTO–TO shows better rate-capability than single phase LTO. Sample LTO–TO exhibits slight difference in specific capacity between 1 C and 2 C rates and presents a higher specific capacity of 134 mA h g^{-1} at 2 C rate, along with a better cycling stability, in contrast with sample LTO. Both samples display good capacity recovery when the charge/discharge rates switch back from 2 C to 0.2 C, suggesting the good intrinsic structure

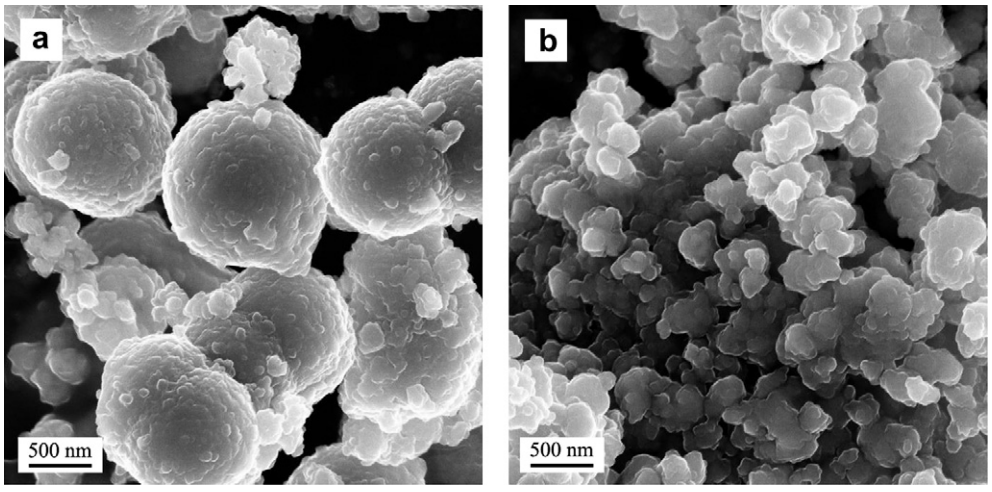

Fig. 2. FESEM images of samples (a) LTO and (b) LTO–TO.

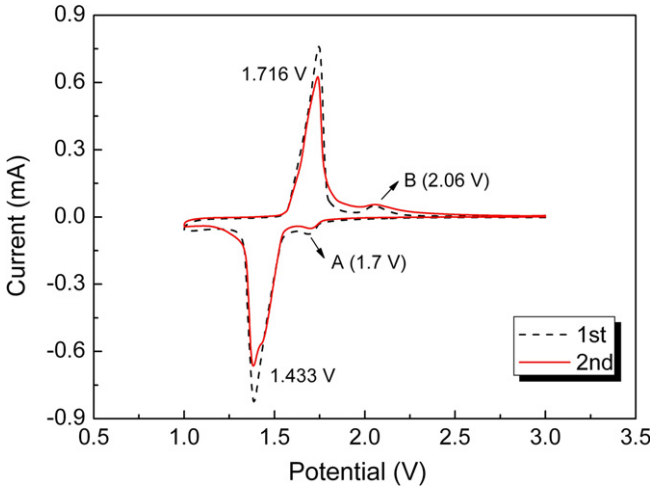

Fig. 4. Cyclic voltammogram of LTO–TO electrode at the scan rate of 0.1 mV s^{-1} between 1.0 and 3.0 V.

stability. The good rate-capability of sample LTO–TO is mainly attributed to its smaller particle size, which effectively reduces the lithium ion diffusion distance during the charge/discharge process and at the same time decreases the local current density due to the high specific surface area [4].

In order to make a better understanding on the contribution of TiO_2 to the electrochemical properties of LTO–TO material, the cyclic voltammogram (CV) test was performed on LTO–TO electrode. The CV results for the first two cycles are shown in Fig. 4. The sharp redox peaks at 1.4 and 1.7 V belong to the lithiation/delithiation processes between $Li_4Ti_5O_{12}$ phase and lithium-rich phase $Li_7Ti_5O_{12}$. The cathodic and anodic peaks centered at 1.7 and 2.06 V, marked as A and B in Fig. 4, are associated with the lithium insertion and removal processes of anatase TiO_2 [30,33], respectively. This indicates that TiO_2 phase is active toward lithiation/delithiation reaction, and thereby can contribute some electrochemical capacity to the LTO–TO electrode.

Considering the facts that the electrode reaction depends on both ionic and electronic conductivity of electrode and decreasing the particle size can only improve the ionic conductivity of electrode, carbon coating strategy is adopted in this work to enhance the electronic conduction of the LTO–TO electrode with the aim of improving further the rate-capability. A 2.5 wt.% carbon was coated on LTO–TO composite by sol–gel and pyrolysis method to prepare LTO–TO/C sample. Fig. 5(a) shows the FESEM image of the LTO–TO/C powder, which presents a uniform particle distribution with the particle size of ca. 200–300 nm. HR-TEM observation reveals that the nano-sized particle has actually core-shell structure, which is composed of two crystal structure phases and an amorphous carbon layer with thickness less than 5 nm on the particle surface, as shown in Fig. 5(b). For the marked regions A and B, the high magnification

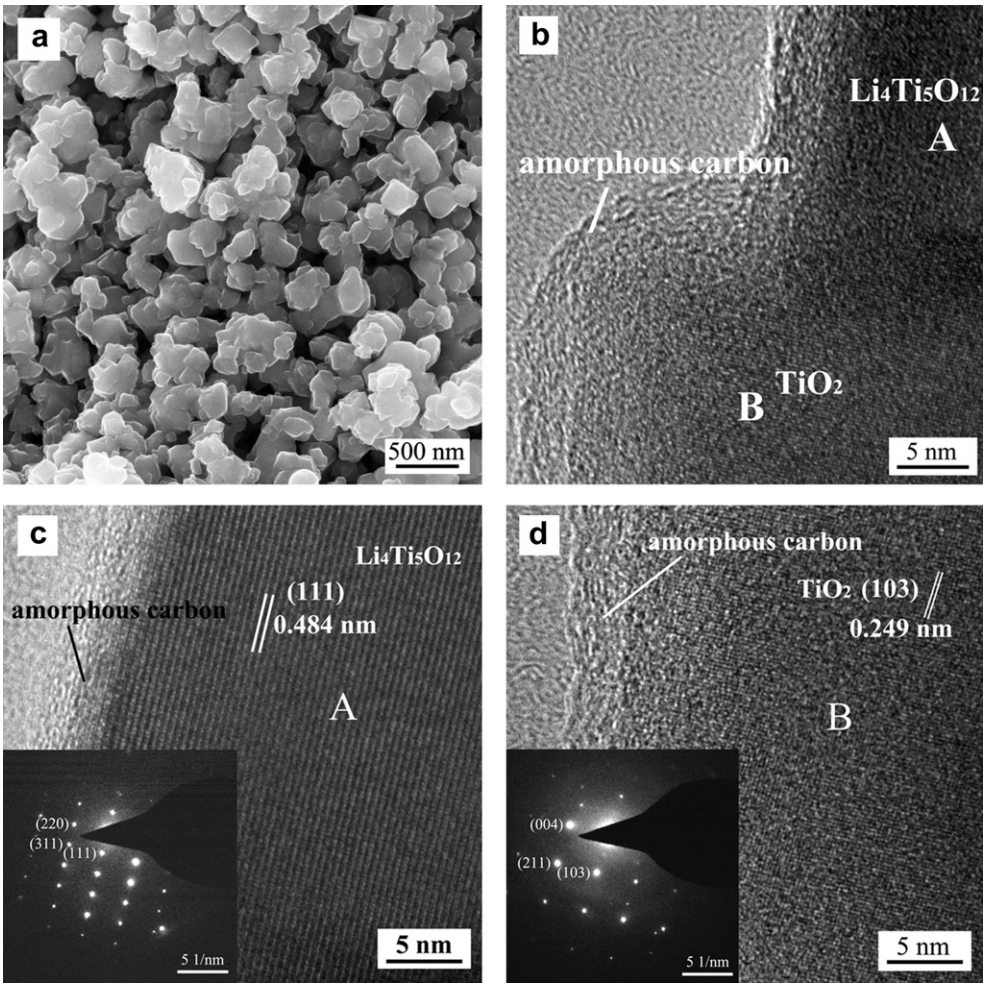

Fig. 5. (a) FESEM image of sample LTO–TO/C; (b) HR-TEM micrograph of sample LTO–TO/C; (c) and (d) HR-TEM micrographs of the area marked as A and B in Fig. 6(b) (inset: selected area diffraction patterns).

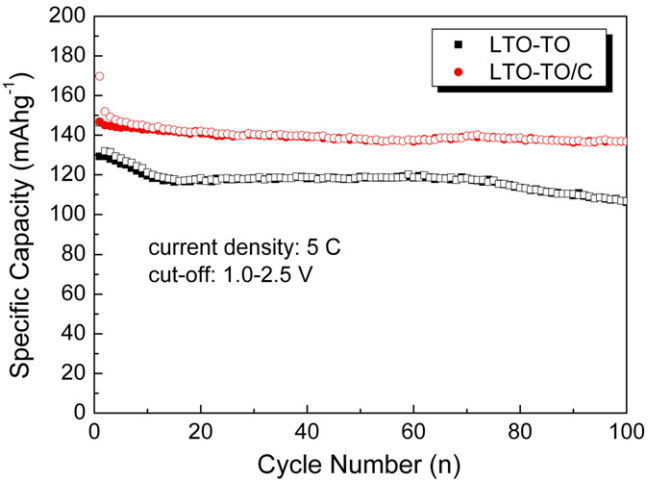

Fig. 6. Cycling performance of samples LTO–TO and LTO–TO/C. Charge/discharge rate: 5 C; cut-off: 1.0–2.5 V.

observation on the lattice spaces combined with the SAED analysis indicates that they are assignable to $Li_4Ti_5O_{12}$ and TiO_2, respectively (Fig. 5(c, d)). The calculated *d*-spacing from the HR-TEM image of A region (Fig. 5(c)) is 0.484 nm, corresponding to the crystal spacing with (111) plane of spinel $Li_4Ti_5O_{12}$. The spacing between contiguous planes in Fig. 5(d) is measured to be 0.249 nm, which matches well with the (103) diffraction plane of anatase TiO_2. An amorphous carbon layer with the thickness less than 5 nm can be clearly observed on the particle surface, which is expected to be favorable for the enhancement of electronic conductivity and thus the rate-capability of electrode.

To examine the effect of carbon coating on the electrochemical performance of LTO–TO anode material, two samples LTO–TO and LTO–TO/C were cycled at 5 C in the potential range of 1.0–2.5 V. The results are presented in Fig. 6. Compared to LTO–TO, the carbon coated sample LTO–TO/C delivers higher reversible specific capacity and better cycling stability. After 100th cycle, sample LTO–TO/C shows the reversible capacity of ~140 mA h g^{-1}, while sample LTO–TO presents only ~110 mA h g^{-1}. The good rate-capability of sample LTO–TO/C is mainly attributed to the carbon coating layer on the particle surface, which enhances the electronic conductivity and thus reduces the electrode polarization. This effect is well reflected in the charge/discharge voltage profiles, as shown in Fig. 7. Sample LTO–TO/C displays very closer and flatter charge/discharge platforms, indicating good electrode kinetics and lower electrode polarization. However, sample LTO–TO exhibits a slope delithiation voltage profile and big gap between the charge and discharge voltage profiles, implying a large electrode polarization. These results demonstrate that LTO–TO/C composite material is a promising anode material for lithium-ion battery.

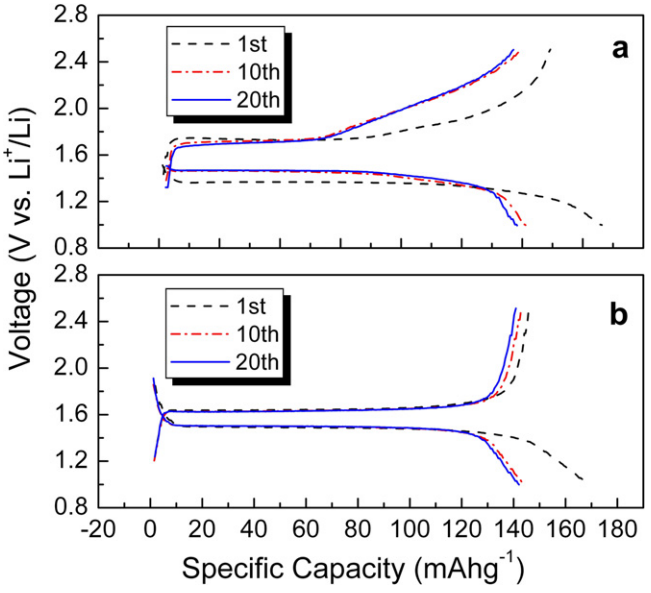

Fig. 7. Charge/discharge voltage profiles of half cells with samples LTO–TO (a) and LTO–TO/C (b) as electrode, respectively. Charge/discharge rate: 5 C; cut-off: 1.0–2.5 V.

4. Conclusions

Single phase $Li_4Ti_5O_{12}$ and dual-phase $Li_4Ti_5O_{12}$–TiO_2 powders were synthesized via solvothermal route. As anode material for lithium ion battery, the *in situ* synthesized $Li_4Ti_5O_{12}$–TiO_2 composite shows higher reversible specific capacity and better rate-capability compared to pure $Li_4Ti_5O_{12}$. The existence of TiO_2 can limit the grain growth and prevent the particle aggregation of $Li_4Ti_5O_{12}$ during synthesis process, thus decreasing the particle size and increasing the contact area between active material and electrolyte solution, which is believed to be favorable for the enhancement of electrode reaction. Moreover, TiO_2 can contribute a certain amount of capacity to the electrode of $Li_4Ti_5O_{12}$–TiO_2. Coating the dual-phase $Li_4Ti_5O_{12}$–TiO_2 composite with carbon can further improve the electrochemical performance. The composite $Li_4Ti_5O_{12}$–TiO_2/C with a thin carbon layer (~5 nm) exhibits an excellent rate-capability, a reversible capacity of ~140 mA h g^{-1} is achieved after 100 cycles at 5 C. The synthesized $Li_4Ti_5O_{12}$–TiO_2/C composite is a promising anode material for power-type lithium ion battery.

Acknowledgments

This work was supported by Program for Guangdong Industry-Academy-Alliance Research (2009A090100020) and Program for New Century Excellent Talents in University of China (NCET-07-0072).

References

[1] J.-M. Tarascon, M. Armand, Nature 414 (2001) 359–367.
[2] B. Dunn, H. Kamath, J.-M. Tarascon, Science 334 (2011) 928–935.
[3] K. Sato, M. Noguchi, A. Demachi, N. Oki, M. Endo, Science 264 (1994) 556–558.
[4] Y.G. Guo, J.S. Hu, L.J. Wan, Adv. Mater. 20 (2008) 2878–2887.
[5] M. Winter, J.O. Besenhard, Electrochim. Acta 45 (1999) 31–50.
[6] M. Winter, J.O. Besenhard, M.E. Spahr, P. Novák, Adv. Mater. 10 (1998) 725–763.
[7] Y. Idota, T. Kubota, A. Matsufuji, Y. Maekawa, T. Miyasaka, Science 276 (1997) 1395–1397.
[8] C.K. Chan, H. Peng, G. Liu, K. McIlwrath, X.F. Zhang, R.A. Huggins, Y. Cui, Nat. Nanotech. 3 (2008) 31–35.
[9] P. Poizot, S. Laruelle, S. Grugeon, L. Dupont, J.-M. Tarascon, Nature 407 (2000) 496–499.
[10] Z.Y. Wang, L. Zhou, X.W. Lou, Adv. Mater. 24 (2012) 1903–1911.
[11] P.L. Taberna, S. Mitra, P. Poizot, P. Simon, J.-M. Tarascon, Nat. Mater. 5 (2006) 567–573.
[12] K.M. Shaju, F. Jiao, A. Débart, P.G. Bruce, Phys. Chem. Chem. Phys. 9 (2007) 1837–1842.
[13] B. Wang, J.S. Chen, H.B. Wu, Z.Y. Wang, X.W. Lou, J. Am. Chem. Soc. 133 (2011) 17146–17148.
[14] D. Bresser, E. Paillard, E. Binetti, S. Krueger, M. Striccoli, M. Winter, S. Passerini, J. Power Sources 206 (2012) 301–309.
[15] E. Ferg, J. Gummow, A. De Kock, M.M. Thackeray, J. Electrochem. Soc. 141 (1994) L147–L150.
[16] T. Ohzuku, A. Ueda, N. Yamamoto, J. Electrochem. Soc. 142 (1995) 1431–1435.
[17] S. Scharner, W. Weppner, P. Schmid-Beurmann, J. Electrochem. Soc. 146 (1999) 857–861.

[18] K. Zaghib, M. Simoneau, M. Armand, M. Gauthier, J. Power Sources 81–82 (1999) 300–305.
[19] K. Ariyoshi, S. Yamamoto, T. Ohzuku, J. Power Sources 119–121 (2003) 959–963.
[20] G.X. Wang, D.H. Bradhurst, S.X. Dou, H.K. Liu, J. Power Sources 83 (1999) 156–161.
[21] C.H. Chen, J.T. Vaughey, A.N. Jansen, D.W. Dees, A.J. Kahaian, T. Goacher, M.M. Thackeray, J. Electrochem. Soc. 148 (2001) A102–A104.
[22] H.L. Zhao, Y. Li, Z.M. Zhu, J. Lin, Z.H. Tian, R.L. Wang, Electrochim. Acta 53 (2008) 7079–7083.
[23] J. Wolfenstine, J.L. Allen, J. Power Sources 180 (2008) 582–585.
[24] T.F. Yi, J. Shu, Y.R. Zhua, X.D. Zhu, C.B. Yue, A.N. Zhou, R.S. Zhu, Electrochim. Acta 54 (2009) 7464–7470.
[25] S.H. Huang, Z.Y. Wen, J.C. Zhang, Z.H. Gu, X.H. Xu, Solid State Ionics 177 (2006) 851–855.
[26] S.H. Huang, Z.Y. Wen, B. Lin, J.D. Han, X.G. Xu, J. Alloys Compd. 457 (2008) 400–403.
[27] G.N. Zhu, H.J. Liu, J.H. Zhuang, C.X. Wang, Y.G. Wang, Y.Y. Xia, Energy Environ. Sci. 4 (2011) 4016–4022.
[28] J.J. Huang, Z.Y. Jiang, Electrochim. Acta 53 (2008) 7756–7759.
[29] L.F. Shen, C.Z. Yuan, H.J. Luo, X.G. Zhang, S.D. Yang, X.J. Lu, Nanoscale 3 (2011) 572–574.
[30] H. Qiao, L.F. Xiao, L.Z. Zhang, Electrochem. Commun. 10 (2008) 616–620.
[31] B. Zachau-Christiansen, K. West, T. Jacobsen, S. Atlung, Solid State Ionics 28–30 (1988) 1176–1182.
[32] Y.Q. Wang, L. Gu, Y.G. Guo, H. Li, X.Q. He, S. Tsukimoto, Y. Ikuhara, L.J. Wan, J. Am. Chem. Soc. 134 (2012) 7874–7879.
[33] M.M. Rahman, J.Z. Wang, M.F. Hassan, D. Wexler, H.K. Liu, Adv. Energy Mater. 1 (2011) 212–220.
[34] C.H. Jiang, Y. Zhou, I. Honma, T. Kudo, H.S. Zhou, J. Power Sources 166 (2007) 514–518.
[35] A.S. Prakash, P. Manikandan, K. Ramesha, M. Sathiya, J.-M. Tarascon, A.K. Shukla, Chem. Mater. 22 (2010) 2857–2863.
[36] T. Ohzuku, Z. Takehara, S. Yoshizawa, Electrochim. Acta 24 (1979) 219–222.